

# Evaluating the control of a DAB converter for an application that involves EV charging using SPS, TPS, DPS, and EPS.

Ali Wassouf, Raj Kumar Saini

**Cite as:** Wassouf, A., & Saini, R. K. (2024). Evaluating the control of a DAB converter for an application that involves EV charging using SPS, TPS, DPS, and EPS. International Journal of Microsystems and IoT, 2(8), 1065–1075. <https://doi.org/10.5281/zenodo.13369536>




© 2024 The Author(s). Published by Indian Society for VLSI Education, Ranchi, India



Published online: 20 August 2024.



Submit your article to this journal: 



Article views: 



View related articles: 



View Crossmark data: 

DOI: <https://doi.org/10.5281/zenodo.13369536>

Full Terms & Conditions of access and use can be found at <https://ijmit.org/mission.php>



# Evaluating the control of a DAB converter for an application that involves EV charging using SPS, TPS, DPS, and EPS.

Ali Wassouf, Raj Kumar Saini

Department of Electronics and Communication Engineering, Shoolini University.

## ABSTRACT

Due to the rising cost of petroleum products and the need to safeguard the environment, electric vehicles are regaining popularity. Internal combustion engines use unidirectional power flow; however, in electrical vehicles, the use of regenerative brakes improves overall process efficiency, necessitating two direction energy flow. This work compares between different control methods and explain how the DPS is the best method. Dual Active Bridge (DAB) are becoming more common because they support power from the grid to the vehicle and from the vehicle to the grid DAB converters have a high-power density, are efficient, and are simple to use. Where triple phase shift (TPS), dual phase shift (DPS), signal phase shift (SPS), and extend phase shift (EPS), regulate DAB converters (TPS). This study analyses various approaches using a MATLAB simulation model for R load and concludes that SPS is the easiest to implement, EPS is better than SPS because of minimal losses, and DPS is the best method because it has two inner phase shifts and TPS is more complicated. Zero voltage switching is simulated for the DAB converter with an R load (SPS).

## KEYWORDS

Zero Voltage Switching, Single-Phase Shift, Triple Phase Shift, Dual-Phase-Shift, Extend Phases Shift.

## 1. INTRODUCTION

Fast chargers charge faster, charge safer, monitor your electricity consumption, optimize charging time, and identify charging stations quickly. In addition to laptops, shavers, and cameras, batteries are used in various applications such as electrical vehicles, the electrical grid, and DC microgrids. Some applications require bidirectional movement to shift power between two DC buses; therefore, a bidirectional converter is appropriate. These items require stable power, so different methods are employed to control the discharging and charging of the battery. To accomplish this, various studies recommend using bidirectional DC-DC and DC-AC converters. Bidirectional converters allow electricity to flow in two directions: forward and reverse, with the load feeding the input and the input feeding the load [1]. Traditional bidirectional converters have low efficiency and large losses, but bidirectional DC/DC converters (digital control) have high performance, soft switching, and high-power densities [2]. Dual active bridge charges EV, while there are difficulties with the dual active bridge during charging and discharging, such as switching losses while charging and discharging [3], high circulating current [4], low efficiency, losses when changing the load [5], and a small range of ZVS [6]. The disadvantage of the DAB is that there is not a large

difference in voltage between the first and second sides of the converter (transformer), so the circulating current will raise the current stress and give us considerable losses. Various approaches for controlling the duty ratio and output voltage are proposed and simulated (SPS, EPS, DPS, and TPS). The output current and voltage will change as the phase delay between the primary and secondary voltages of the transformer changes. Dual active bridge has two bridges, each with four switches, with a high frequency transformer and inductor, and the most important thing is the outer phase shift between the primary and secondary bridges [7].

When SPS is employed, the first bridge requires two pulses, while the second bridge requires two pulses [8]. When EPS is used, the first bridge requires four pulses and two pulses for the second bridge [9]. For DPS and TPS, four pulses for the first bridge and four pulses for the second bridge are required [10].

Zero voltage switching (ZVS) is a technique used in DAB converters to minimize switching losses and improve the efficiency of the converter [11]. In a DAB converter, two active switches are used to regulate the flow of current through the primary winding of a transformer. By carefully controlling the switching times of these active switches, it is possible to achieve ZVS, where the voltage across the switches is nearly zero when they are turned on or off [12].

This helps to minimize the power losses associated with the switching process and results in a more efficient converter. Additionally, ZVS can also reduce the stresses on the active switches and improve the reliability of the converter [13].

This paper compares the control system methods of dual active bridge, showing which one is the best method and zero voltage switching achieved in case of SPS.

The paper is laid out in fallows. The first section's introduction. Section 2 describes a dual active bridge, control approach and power flow in a dual active bridge. Section 3 explains the zero-voltage switching in the converter. Section 4's simulation section and Section 5's conclusion.

## 2. Dual Active Bridge

The dual active bridge is used in a variety of appliances, including electric vehicles (EV), uninterruptible power supplies (UPS), and microgrid systems Using this charger provides a quick dynamic response and high effectiveness [14].

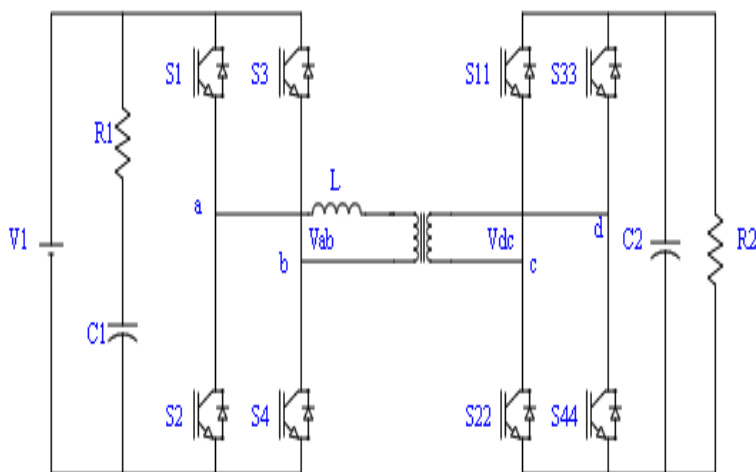


Fig 1. A Dual Active Bridge

A DAB is a sort of power converter that is used to shift power from one source to another. It is a bi-directional converter, meaning it can accept and deliver power in either way [15]. As a result, the DAB is an important component in many renewable energy systems, comprising wind turbines and solar panels, where it can be utilised to transfer power from the renewable energy source to the grid or to a storage system [16].

Dual active bridge: two bridges linked with a transformer in the forward direction, where the primary bridge flips DC to AC and the secondary bridge flips AC to DC [17]. The primary bridge operates at 50% duty cycle, producing  $V_{ab}$  (The voltage of the first bridge), and the second bridge operates at 50% duty cycle with  $V_{dc}$  input. where the DAB can be controlled in various methods such as (TPS, EPS, SPS, and DPS) [18]. Figure 1 illustrates a DAB.

### 2.1 Single Phase Shift (SPS)

SPS is the most employed control approach in DAB, as illustrated in Fig. 2. S1–S4 and S11–S44 are fifty-percent duty ratio square-wave gate impulses. Where  $V_{dc}$  and  $V_{ab}$  are the output voltages of the first and second bridge, respectively [19]. In SPS, the cross-switches in each bridge are shifted together to create impulses with a fifty-percent duty ratio. The voltage across the leaking inductor changes when the phase delay between  $V_{ab}$  and  $V_{dc}$  changes. So, the power flow value can then be inductor changes when the phase delay between  $V_{ab}$  and  $V_{dc}$  changes. So, the power flow value can then be regulated [20]. SPS has received a lot of attention since it has many features such as low inertia, rapid dynamic, and simple soft switching implementation. As a result, energy loss will rise while efficiency will fall [21].

### 2.2 Extended Phase Shift (EPS)

EPS is an upgraded technique of SPS in which cross-switches in one bridge are shifted in turn while cross-switches in another bridge are shifted with an internal phase delay [22]. As a result, the output of the bridge's internal phase shift becomes 3 levels, while the other is 2 levels with a fifty percent duty ratio. The energy that flows back during the mean duration of zero voltage in 3-levels is zero; hence, the circuiting power will decrease [23]. When EPS is compared to SPS, in addition to the exterior phase shift in EPS is the phase delay between  $V_{ab}$  and  $V_{dc}$ , and the internal phase delay is the phase shift in one bridge between pulses. Whereas external phase shift is employed to adjust the direction and amplitude of energy flow, internal phase delay is employed to minimise circulating power and extend the ZVS region [24].

Table 1 comparing between control methods.

## 2.3 Dual Phase Shift (DPS)

Control method	Regulation Degree	The first bridge's output level (AC)	The second bridge's output level (AC)	Remarks
SPS	1. $\phi$	2 levels	2 levels	<ul style="list-style-type: none"> <li>Using the SPS with the PI controller improves DAB reliability [30].</li> <li>According to SPS, the switch stress is at its highest in DAB [31].</li> <li>Under SPS management, full load is possible in region ZVS [32].</li> <li>Quick dynamic, low inertia, and ease of implementing soft switching control are advantages of SPS control [33].</li> </ul>
EPS	1. $\phi$ 2.D	3 levels	2 levels	<ul style="list-style-type: none"> <li>In [34], EPS is used to regulate DAB, with the ZVS dividing into two portions.</li> <li>EPS can be utilised for heavy loads [35].</li> <li>The energy transfer is regulated by <math>\phi</math> and D under EPS [36].</li> <li>In DAB, the EPS technique is employed to lower the peak current throughout the entire power range [37].</li> </ul>
DPS	1. $\phi$ 2.D	3 levels	3 levels	<ul style="list-style-type: none"> <li>Relative to the SPS, the DPS can provide a larger power transmission region [38].</li> <li>DPS has smaller loss as compared to EPS [39].</li> <li>By employing DPS, the reverse energy flow is reduced [40].</li> <li>DPS is a simple, implementable model [41].</li> </ul>
TPS	1. $\phi$ 2.D1 3.D2	3 levels	3 levels	<ul style="list-style-type: none"> <li>TPS is employed to enhance efficiency, decrease reactive power, and decrease current pressure [42].</li> <li>Due to the extra degree of freedom in regulating the transformer current, the DAB TPS offers smooth switching across the whole power flow range [43].</li> <li>TPS is used in a reactive power reduction method for high power DAB converters [44].</li> <li>TPS has three control degrees <math>\phi</math>, D1 and D2 [45].</li> </ul>

In DPS, there is an external phase delay between the first and second bridge and an internal phase delay in every bridge. So, the output AC of both bridges is 3-levels [25]. In comparison to SPS, DPS can lower fault currents, improve efficiency, widen the ZVS region, and decrease output capacitance. In comparison to DBS, EPS is easier to implement and provides better rendering [26].

**2.4 Triple Phase Shift (TPS)**

Each bridge has an internal phase shift, and these two internal phase shifts are different on each other [27]. The TPS control method was introduced after SPS, EPS [28]. According to Table 1, SPS requires only 1 control level, DPS and EPS require 2 control levels, and TPS requires 3 control levels. As a result, TPS is the most challenging to implement. In terms of development difficulties and efficiency, DPS control may be the relative best solution for large-scale practical implementation [29]. Table 1 compares control approaches, while figures 2, 3, 4, and 5 depict SPS, EPS, DPS, and TPS separately.

**2.5 Power flow regulation in a dual active bridge**

The analysis and performance of a DAB have been explored in, where figure.6 demonstrates that the amplitude and direction of energy flow can be changed by adjusting the phase delay between the first and second bridge's AC output voltages, Vab and Vdc. Transmission energy concepts of trinalational AC power systems and DAB can be driven as follows:

$$P_{sine} = \frac{V_{rms1}V_{rms2}}{2\pi fsL} * \sin\phi$$

$$P_{square} = \frac{nV1V2}{2\pi^2 fsL} (\pi - \phi) * \phi$$

where  $V_{rms1}$  and  $V_{rms2}$  are the RMS values of a sinusoidal wave and  $\phi$  is the phase delay between the output of two bridges. The energy output enhances due to high-frequency power transmission. Figure 6 depicts the basic circuit of a DAB.

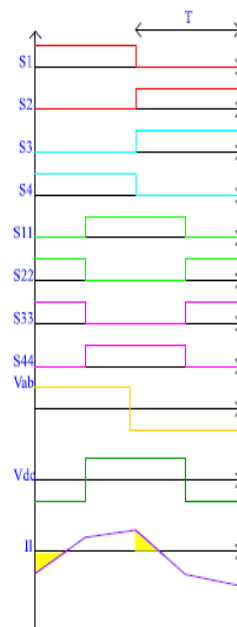


Fig. 2. Single Phase Shift



Fig. 3. Extended Phase Shift



Fig. 4. Dual Phase Shift

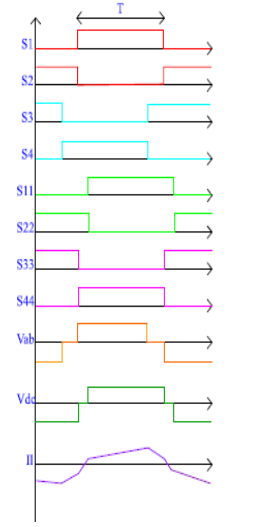


Fig. 5. Triple Phase Shift

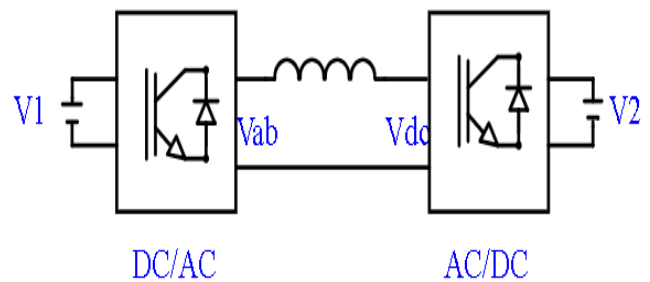


Fig. 6 Basic circuit of dual active bridge.

### 3. Zero voltage switching

Under normal conditions, one of the features of the DAB is soft switching of all devices. However, the ZVS may be lost if the power delivered by DAB is reduced, especially on the second bridge. ZVS loss not only reduces efficiency but also increases device noise. The value of the current via the leakage inductor at two crucial points is extremely relevant. These two points represent the current through  $L_k$  when the first and second bridges are exchanged. These two current values are represented in Figure 7 (a) and (b). This ensures that current can flow through the

diode of the transistors to offer soft switching. Figure 7 shows the ideal phase shift regulation operational waveform.

Describing the relationship between DAB's output and input voltage as follows:

$$M = \frac{v_o}{v_i n} \tag{1}$$

$I_1$  and  $I_2$  can be expressed as follows [50]:

$$I_1 = \frac{T v_i}{2 L_k} (2 M d + 1 - M) \tag{2}$$

$$I_2 = \frac{T v_i}{2 L_k} (2 d - 1 + M) \tag{3}$$

- When  $M=1$ ,  $I_1 = I_2$ , and greater than 0 for the positive phase shift value.

$$I_1 = \frac{T}{L_k} * v_i d \tag{4}$$

$$I_2 = \frac{T}{L_k} * v_i d \tag{5}$$

$T$  is one-half of the switching period;  $d$  is the phase difference between  $v_1$  and  $v_2$ ;  $L_k$  leakage inductor.

- When  $M < 1$ , the required condition for obtaining the ZVS in the second bridge, is met by this expression:

$$d > \frac{1-M}{2}, \quad I_1 > 0.$$

The following formula is employed to ensure the ZVS in the first bridge:

$$d > \frac{M-1}{2M}$$

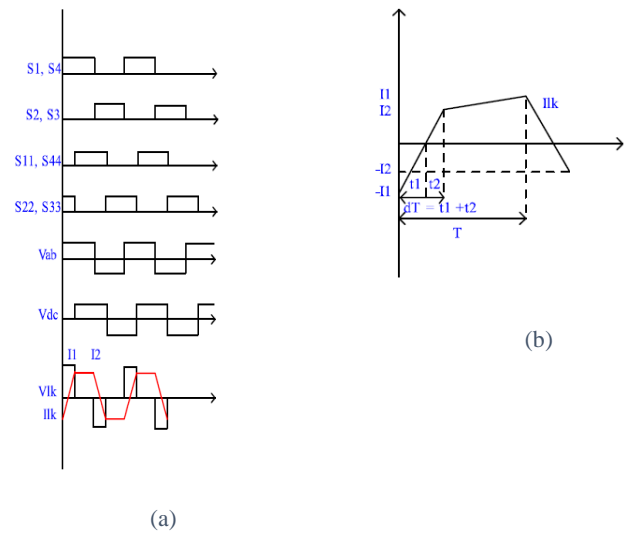


Fig. 7. The optimal operating waveform of the phase shift regulation.

### 3. Simulation

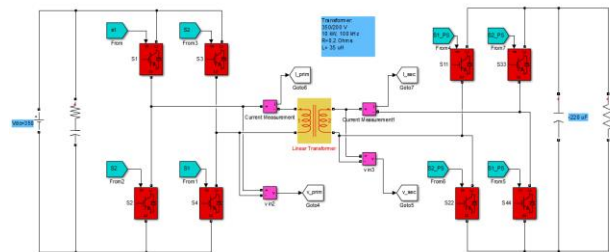


Fig. 8. Simulation of dual active bridge

The intended DAB is simulated in MATLAB with a nominal power of 10 kw and a frequency of 100 kHz. Figure 8 depicts the DAB's simulated performance, where G1, G2 are gate pulses to S1-S4 and G11, G22 are gate pulses to S11-S44. The input dc voltage is 350V with 0.001 Ohm and 220e-6 F for resistor and capacitor respectively. Table 2 provides information on the parameters of the DAB, and Table 3 displays the values of the transformer.

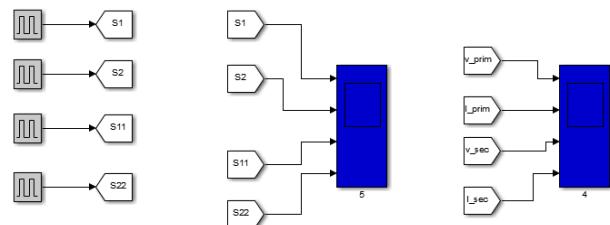


Fig. 9. Single phase shift

Figure 9 depicts the control system of the DAB by SPS. The pulses were generated using four pulse generators. This method is quite basic and simple. Tables 2 and 3 were utilised as parameters for all control systems. The phase angle between pulses is shown in table 4. In SPS, the phase shift of S1 and S4 is zero, while the phase shift of S2 and S3 is 180. As the phase shift of S11 and S44 is 90, there is a outer phase shift between the pulses of the first and second bridges. In EPS, the phase shifts of S1–S4 are in different positions due to the inner phase shift. However, S11-S44 is the same as SPS. In DPS, the phase shifts of S1-S4 and S11-S44 are in different positions due to the inner phase delay in the first and second bridges, which is the same inner phase delay. In TPS, there are two different inner phase shifts in the first and second bridges.

Table 1 Parameter of dual active bridge

Input voltage	350V
Output voltage	200V
R1	0.001 Ohm
C1	220e-6 F
R2	20 Ohm
C2	220e-6 F

Table 2 parameter of transformer

Transformer
350/200V
10KW,100kHz
R = 0.2 Ohm
L = 35uF
Magnetization resistance = 5000 Ohm
Magnetization inductance = 150.16 Ohm

Table 3 phase angle of control methods

	S1	S2	S3	S4	S11	S22	S33	S44
SPS	0	180	180	0	90	270	270	90
EPS	0	180	252	72	90	270	270	90
DPS	72	252	216	36	126	306	270	90
TPS	90	270	216	36	126	306	270	90

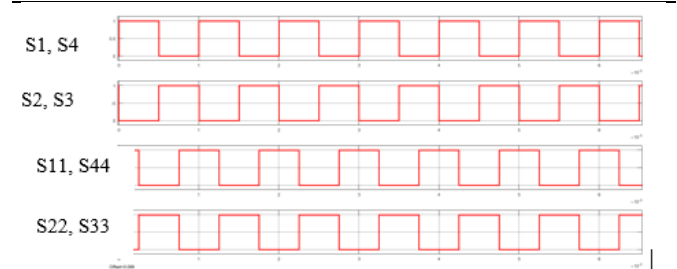


Fig. 10 Single phase shift

Figure 10 shows four pulses for two bridges. For a pulse generator block, the amplitude is 1, the period is  $1/f = 1/100\ 000\text{H} = 0.0001\ \text{s}$ , and the pulse width is 50% of the period. But the phase delay is 0, 0.000005, 0.0000075, and 0.0000025. From this figure, we can see the outer phase delay between the first and second pulses.

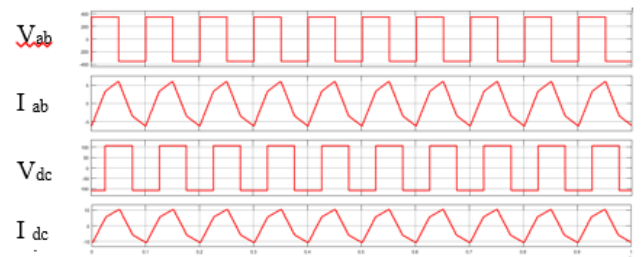


Fig. 11 Parameters of the transformer in the case of SPS.

Figure 11 shows the ac outputs of the transformer are two-level. with a phase shift between these voltages. The primary and secondary currents have the same shape, which indicates that four different voltages apply to the inductor. Figure 12 displays the output voltage and current of a DAB.

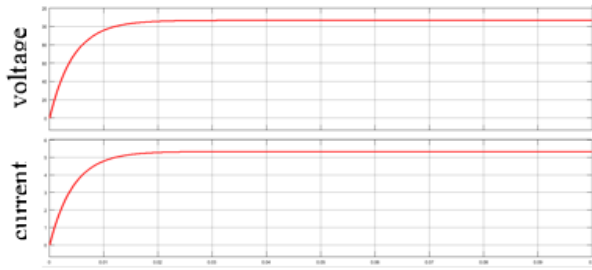


Fig. 12 Output current and voltage in the case of SPS.

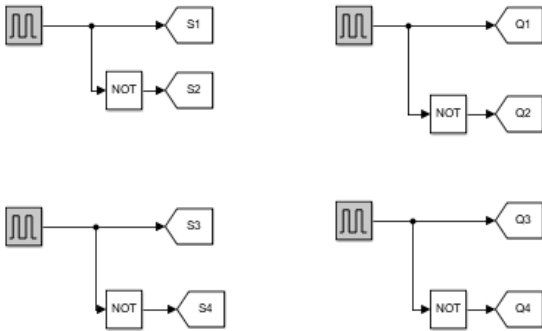


Fig. 13 Extend phase shift.

Figure 13 depicts the control system of the dual active bridge by EPS. G1 will generate pulses for S1 and S2, while G2 will generate pulses for S3 and S4. According to the second bridge, G11 will generate pulses for S11 and S22, while G22 will generate pulses for S33 and S44.

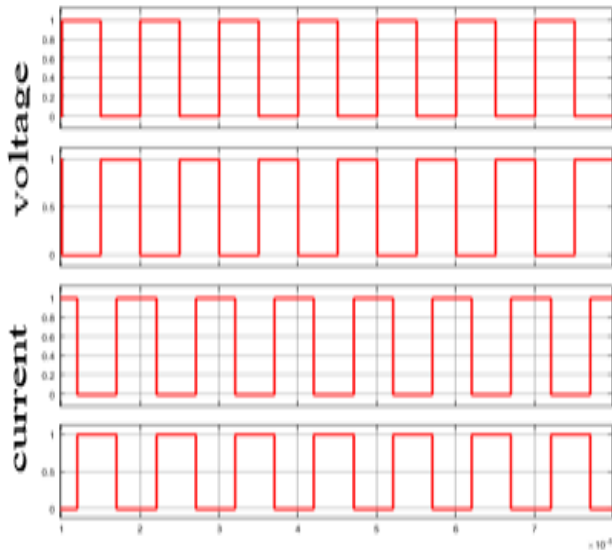


Fig. 14 The pulses of first bridge EPS.

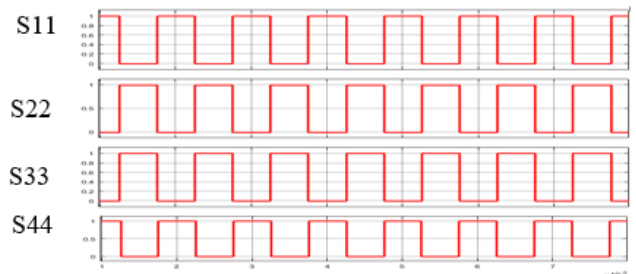


Fig. 15 The second bridge pulses EPS.

Figures 14 and 15 show the pulses of the first and second bridges, respectively. The phase delay is 0, 0.000007, 0.0000075, and 0.0000025. All other parameters are the same as SPS. There is an outer phase delay between primary and secondary bridge pulses and only an inner phase delay in the first bridge.

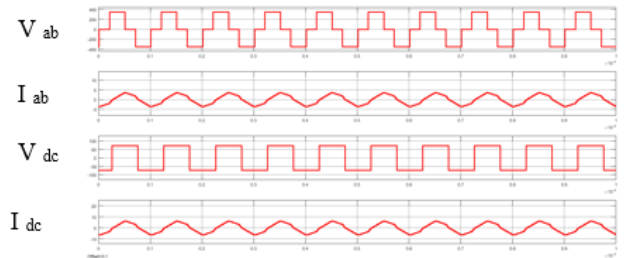


Fig. 16 Parameters of transformer in the case of EPS.

Figure 16 shows the ac outputs of the transformer, first bridge with 3-level voltage and second bridge with 2-level voltage. Figure 17 displays the output voltage and current of a dual-active bridge in the case of EPS.

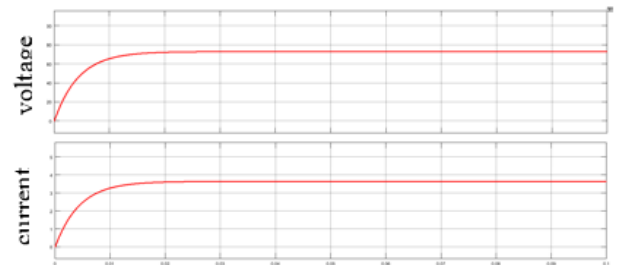


Fig. 17 Output current and voltage in the case of EPS.

The control system of DAB by DPS is same as EPS in Figure 13 with phase delays of 0.000002, 0.000006, 0.0000075, and 0.0000035. All other parameters are the same as SPS.



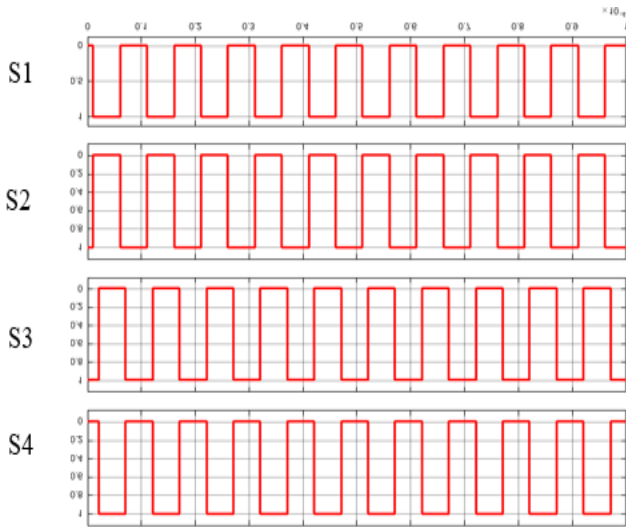


Fig. 18 The pulses of first bridge DPS.

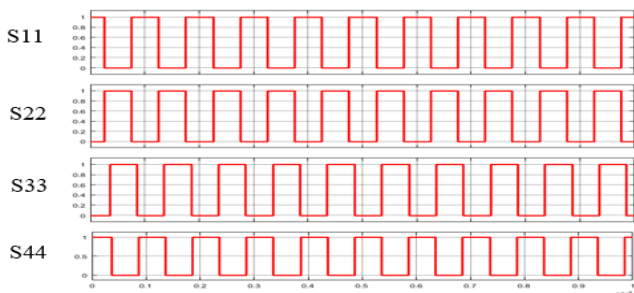


Fig. 19 The second bridge pulses DPS.

Figures 18 and 19 show the pulses of the primary and secondary sides of the bridge, with an outer phase delay between the primary and secondary bridge pulses and the same inner phase delay on both sides of the bridge.

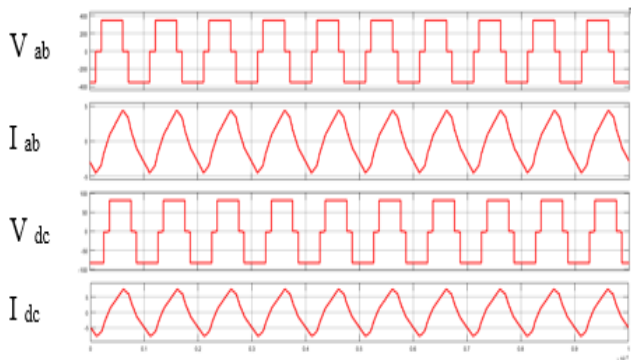


Fig. 20 Parameters of transformer in the case of DPS.

Figure 20 depicts the voltage on both sides of the transformer, which is at three levels. Figure 21 displays the output voltage and current of a dual-active bridge in the case of DPS.

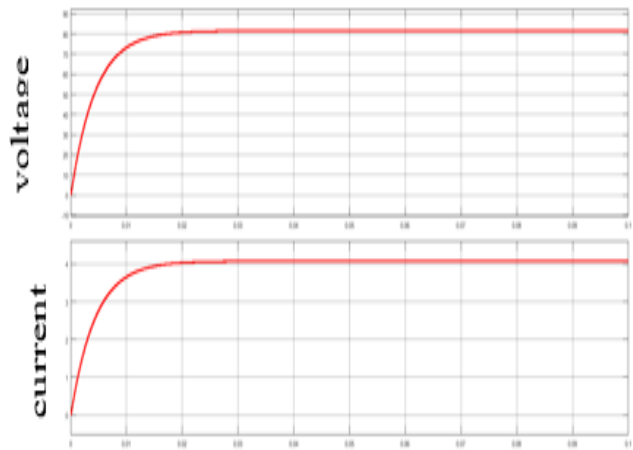


Fig. 21 Output current and voltage in the case of DPS.

The control system of the DAB by TPS is the same as EPS in figure 13, with phase delays of 0.0000025, 0.000006, 0.000001, and 0.0000035.

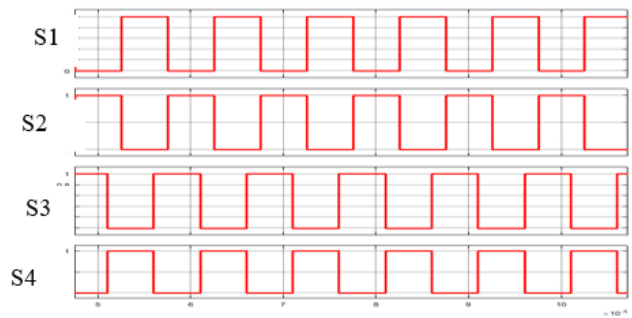


Fig. 22 The pulses of first bridge TPS.

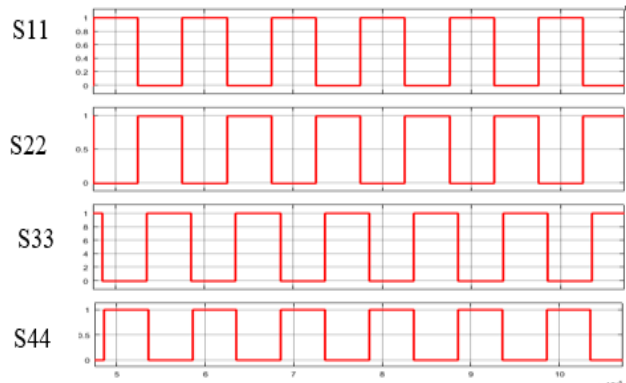


Fig. 23 The second bridge pulses TPS.

Figures 22 and 23 show the pulses of the first and second sides of the bridge, with an outer phase delay between the first and second bridge pulses and a different inner phase delay on both sides of the bridge.

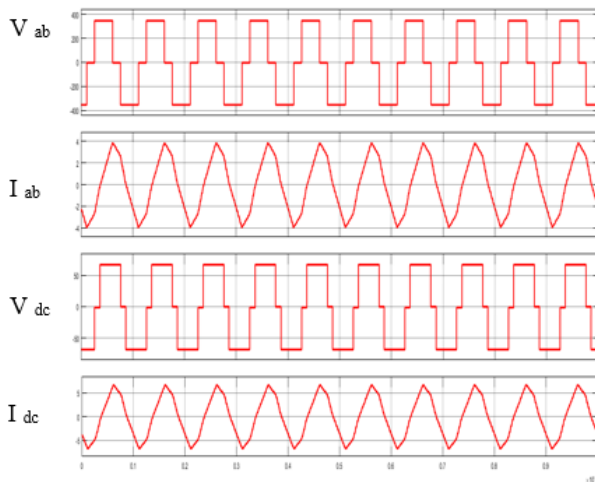


Fig. 24 Parameters of transformer in the case of TPS.

Figure 24 depicts the transformer's alternating current outputs; both sides of the transformer have three levels of voltage. Figure 25 displays the output voltage and current of a DAB in the case of TPS.

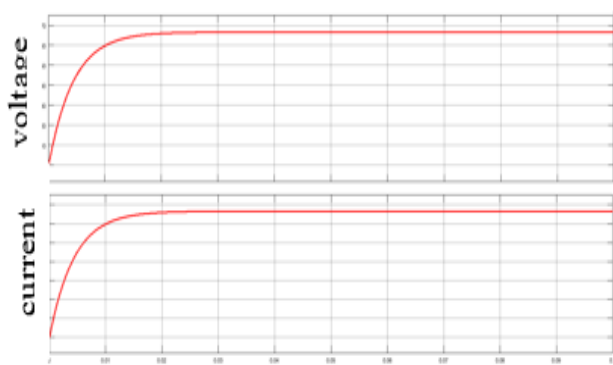


Fig. 25 Output current and voltage in the case of TPS.

#### 4. CONCLUSION

The control methods of DAB, DPS, EPS, SPS and TPS have been investigated in this study. The functioning principle of DAB, which is connected to a resistor, was evaluated using MATLAB. According to the findings of a study, SPS is the simplest to use, EPS is superior to SPS because of minimal losses, and DPS is the best approach because it has two inner phase shifts, while TPS is more difficult. conclusion that SPS is the simplest to use, EPS is superior to SPS because of minimal losses, and DPS is the best approach because it has two inner phase shifts while TPS is more difficult. For the DAB, zero voltage switching is emulated with an R load (SPS). This work compares between different control methods and explain how the DPS is the best method.

#### REFERENCES

- Goel A. & Singh G. (2013). A Novel Low Noise High Gain CMOS Instrumentation Amplifier for Biomedical Applications. *International Journal of Electrical and Computer Engineering*, 3(4), 516-52. <http://dx.doi.org/10.11591/ijece.v3i4.3170>
- Razzavi B. (2012) Design of Analog CMOS Integrated Circuit. Tata McGraw Hill Education.
- Thomas Kugelstadt. (2005). Getting the most out of your instrumentation amplifier design, *Analog Applications Journal*. Texas Instruments Incorporated, Texas, USA, 25-30. <https://www.ti.com/lit/pdf/slyt226>
- Tang, A. T. K. (2005). Enhanced programmable instrumentation amplifier, *SENSORS*, IEEE, Irvine, CA, USA, 1-4. <https://doi.org/10.1109/ICSENS.2005.1597859>
- Analog Devices. (2006). Programmable Gain Instrumentation amplifier AD625, One Technology Way, C00780c-0-6/00 (rev. D), 1-15. <https://www.analog.com/media/en/technical-documentation/data-sheets/ad625.pdf>
- Kultgen M. (2005). Simple, Precise Instrumentation Amplifier Features Digitally Programmable Gains from 1 to 4096. *Analog Devices, Linear Technology Magazine*, 16-19. <https://www.analog.com/en/technical-articles/simple-precise-instrumentation-amplifier-features-digitally-programmable-gains.html>
- Fortunado K. (2018). Programmable Gain Instrumentation Amplifier: Find the best amplifier for you, *Analog Dialogue*, 52, 1-6. <https://www.analog.com/en/analog-dialogue/articles/programmable-gain-instrumentation-amplifiers-finding-one-that-works-for-you.html>
- Mourya S., Naik P. & Sharma P. (2013). Designing of Current Mode Instrumentation Amplifier for Bio-Signal Using 180nm CMOS Technology. *International Journal of Engineering Research & Technology (IJERT)*, 2(4), 2529-2534. <https://doi.org/10.17577/IJERTV2IS4947>
- Roy S. C. D. (1984). Digitally Programmable Gain Amplifiers. *IEEE Transactions on Instrumentation and Measurement*, 33 (4), 329-332. <https://doi.org/10.1109/TIM.1984.4315234>
- Vyroubal D. (1990). Instrumentation amplifier with digital gain programming and common-mode rejection trim. *IEEE Transactions on Instrumentation and Measurement*, 39(4), 588-593 <https://doi.org/10.1109/19.57238>
- Di Ciano M., Tangorra R. & Marzocca C. (1996). Designing a low cost, low noise programmable gain instrumentation amplifier. *Proceedings of 8th Mediterranean Electrotechnical Conference on Industrial Applications in Power Systems, Computer Science and*

- Telecommunications (MELECON 96), 3, 1263-1266. <https://doi.org/10.1109/MELCON.1996.551175>
12. Schaffer V., Snoeij M. F., Ivanov M. V. & Trifonov D. T. (2009). A 36 V Programmable Instrumentation Amplifier with Sub-20  $\mu\text{V}$  Offset and a CMRR in Excess of 120 dB at All Gain Settings. *IEEE Journal of Solid-State Circuits*, 44, 2036-2046. <https://doi.org/10.1109/JSSC.2009.2021921>
  13. Mahmoud S. A. and Alhammadi A. A. (2015). A CMOS digitally programmable OTA based instrumentation amplifier for EEG detection system. 2015 IEEE International Conference on Electronics, Circuits, and Systems (ICECS), 543-546. <https://doi.org/10.1109/ICECS.2015.7440374>
  14. Adimulam M. K., Movva K. K., Kolluru K. and Srinivas M. B. . (2017). A 0.32  $\mu\text{W}$ , 76.8 dB SNDR Programmable Gain Instrumentation Amplifier for Bio-Potential Signal Processing Applications. 2017 IEEE Computer Society Annual Symposium on VLSI (ISVLSI), 655-660.
  15. Schoeneberg U., Hosticka B. J. & Schnatz F. V. (1991). A CMOS readout amplifier for instrumentation applications. *IEEE Journal of Solid-State Circuits*, 26(7) 1077-1080. <https://doi.org/10.1109/4.92029>
  16. Menolfi C. & Huang Qiuting. (1999). A fully integrated, untrimmed CMOS instrumentation amplifier with submicrovolt offset. *IEEE Journal of Solid-State Circuits*, 34(3), 415-420. <https://doi.org/10.1109/4.748194>
  17. Eldeeb M. A., Ghallab Y. H., Ismail Y. & El ghitani H. (2016). Design of low power CMOS subthreshold current mode instrumentation amplifier based on CCII. 2016 IEEE 59th International Midwest Symposium on Circuits and Systems (MWSCAS), Abu Dhabi, 1-4. <https://doi.or/10.1109/MWSCAS.2016.7870137>
  18. Ren M., Zhang C.X. & Sun D. S. (2012). Design of CMOS Instrumentation Amplifier. *Procedia Engineering*. 29, 4035-4039(Vol. 29). <https://doi.org/10.1016/j.proeng.2012.01.615>
  19. Gupta G. & Tripathy M. R. (2014). CMOS Instrumentation amplifier design with 180nm technology. 2014 International Conference on Circuits, Power and Computing Technologies [ICCPCT-2014], Nagercoil, India, 1114-1116. <https://doi.org/10.1109/ICCPCT.2014.7055007>
  20. Bardyn J., Kaiser A. & Stefanelli B. (1990). A Very Low-Noise Instrumentation Amplifier using a Standard CMOS Process for Digital Chips. *ESSCIRC '90: Sixteenth European Solid-State Circuits Conference*, Grenoble, France, 29-32.
  21. Nielsen J.H., & Bruun E. (2004). A CMOS Low-Noise Instrumentation Amplifier Using Chopper Modulation. *Analog Integr Circ Sig Process*, 42, 65–76. <https://doi.org/10.1007/s10470-004-6849-8>
  22. Saurabh S., Saifi M., Karatangi S.V., & Rai A. (2020). Design of CMOS Instrumentation Amplifier Using Three-Stage Operational Amplifier for Low Power Signal Processing. In: G.Mathur, H.Sharma, M. Bunde, N. Dey, M. Paprzycki (eds) *International Conference on Artificial Intelligence: Advances and Applications 2019. Algorithms for Intelligent Systems*. Springer, Singapore. [https://doi.org/10.1007/978-981-15-1059-5\\_9](https://doi.org/10.1007/978-981-15-1059-5_9)
  23. Eldeeb M. A., Ghallab Y. H., Ismail Y. & El Ghitani H. (2018). An 89 nW instrumentation amplifier for IoT in 65 nm CMOS technology. 2018 35th National Radio Science Conference (NRSC), Cairo, Egypt, 345-351, <https://doi.org/10.1109/NRSC.2018.8354394>
  24. Wu R., Huijsing J.H., & Makinwa K.A.A. (2011). A Current Feedback Instrumentation Amplifier with a Gain Error Reduction Loop and 0.06 % Untrimmed Gain Error. *IEEE Journal Solid State Circuits*, 46(12), 2794-2806. <https://doi.org/10.1109/JSSC.2011.2162923>
  25. Eldeeb M. A., Ghallab Y. H., Ismail Y. & El ghitani H. (2016). Design of low power CMOS subthreshold current mode instrumentation amplifier based on CCII. 2016 IEEE 59th International Midwest Symposium on Circuits and Systems (MWSCAS), Abu Dhabi, 1-4. <https://doi.org/10.1109/MWSCAS.2016.7870137>
  26. Goel V., Surshetty S. K., Prasad D. & Nath V. (2019),. Design of an Area Efficient and High-gain CMOS Instrumentation Amplifier for VLSI Applications. 2019 *Innovations in Power and Advanced Computing Technologies (i-PACT)*, Vellore, India, 1-6. <https://doi.org/10.1109/i-PACT44901.2019.8960230>
  27. Worapishet A., Demosthenous A. & Liu X. (2011). A CMOS Instrumentation Amplifier With 90-dB CMRR at 2-MHz Using Capacitive Neutralization: Analysis, Design Considerations, and Implementation. *IEEE Transactions on Circuits and Systems I: Regular Papers*, 58(4), 699-710 <https://doi.org/10.1109/TCSI.2010.2078850>
  28. Venkata Krishna O. et. al. (2015). Design and Implementation of Instrumentation Amplifier for EEG in 180nm CMOS technology. *CVR Journal of Science and Technology*, 8, 57-64. <http://dx.doi.org/10.32377/cvrjst0811>
  29. Sanjay, R., Venkataramani, B., Kumaravel, S. et al. (2021). A Low-Noise Area-Efficient Current Feedback Instrumentation Amplifier. *Circuits Syst Signal Process*, 40, 1496–1510. <https://doi.org/10.1007/s00034-020-01527-2>.
  30. Minch B. A. (2017). A CMOS differential-difference amplifier with class-AB input stages featuring wide differential-mode input range. 2017 IEEE International

- Symposium on Circuits and Systems (ISCAS), 1-4. <https://doi.org/10.1109/ISCAS.2017.8050488>
31. Riem R., Raman J., Borgmans J. & Rombouts P. (2021). A Low-Noise Instrumentation Amplifier with Built-in Anti-Aliasing for Hall Sensors, in IEEE Sensors Journal, 21(17), 18932-18944., <https://doi.org/10.1109/JSEN.2021.3090251>
  32. F. Neves, J. P. Oliveira & H. Oliveira (2021), A sub-1V CMOS Instrumentation Amplifier for an AFE Interfacing with Sensors, 2021 International Young Engineers Forum (YEF-ECE), 1-6. <https://doi.org/10.1109/YEF-ECE52297.2021.9505076>
  33. Fan Q., Huijsing J. H. & Makinwa K. A. A. (2012). A 21 nV/ $\sqrt{\text{Hz}}$  chopper stabilized multi-path current-feedback instrumentation amplifier with 2  $\mu\text{V}$  offset. IEEE J. Solid-State Circuits, 47(2), 464-475. <https://doi.org/10.1109/JSSC.2011.2175269>
  34. Lin T. N., Wang B., Belhaouari S. B. & Bermak A. (2020). A Chopper Instrumentation Amplifier with Amplifier Slicing Technique for Offset Reduction. 2020 IEEE International Symposium on Circuits and Systems (ISCAS), 1-5. <https://doi.org/10.1109/ISCAS45731.2020.9180507>
  35. Peddiraju B., Jatoth R. K. & Duggirala N. (2014). Performance Comparison of Instrumentation Amplifiers – A Beginner's View, International Conference on Data Data Acquisition, Transfer, Processing & Management [ICDATPM-2014], 138-143. <https://doi.org/10.13140/2.1.4709.6966>
  36. Sankaran K. S. & Purushothaman K. E. (2017). Adaptive Enhancement of Low Noise Amplifier Using Cadence Virtuoso Tool. 2017 Second International Conference on Recent Trends and Challenges in Computational Models (ICRTCCM), 330-334, <https://doi.org/10.1109/ICRTCCM.2017.37>
  37. Ivanov E. V. (2012). Switched-capacitor level-shifting technique with sampling noise reduction for rail-to-rail input range instrumentation amplifiers, IEEE Trans. on Cir. and Sys.-I, 59(12), 2867-2880. <http://dx.doi.org/10.1109/TCSI.2012.2206455>
  38. Serra H., Bastos I., de Melo J. L. A., Oliveira J. P., Paulino N., Nefzaoui E., & Bourouina T. (2019). A 0.9-V Analog-to-Digital Acquisition Channel for an IoT Water Management Sensor Node. IEEE Transactions on Circuits and Systems, 66(10), 1678-1682. <https://doi.org/10.1109/TCSII.2019.2933276>
  39. Yaul F. M. & Chandrakasan A. P. (2017). A noise-efficient 36 nV/ $\sqrt{\text{Hz}}$  chopper amplifier using an inverter-based 0.2-V supply input stage. IEEE J. Solid-State Circuits, 52(11), 3032-3042. <https://doi.org/10.1109/JSSC.2017.2746778>
  40. Lin T. N., Wang B. & Bermak A. (2018). Review and Analysis of Instrumentation Amplifier for IoT Applications, 2018 IEEE 61st International Midwest Symposium on Circuits and Systems (MWSCAS), 2018, 258-261, <https://doi.org/10.1109/MWSCAS.2018.8623882>
  41. Yazicioglu R. F., Merken P., Puers R., & Hoof C. V. (2007). A 60 W 60 nV Hz readout front-end for portable biopotential acquisition systems. IEEE J. Solid-State Circuits, 42(5), 1100-1110. <https://doi.org/10.1109/JSSC.2007.894804>
  42. Kaushik R., & Kaur J. (2021). Design of folded cascode op amp and its application – bandgap reference circuit. Circuit World., 101, 182-191. <https://doi.org/10.1108/CW-10-2019-0137>
  43. Sharma D., Rai A., Debbarma S., Prakash O., Ojha M K & Nath V. (2023). Design and Optimization of 4-Bit Array Multiplier with Adiabatic Logic Using 65 nm CMOS Technologies, IETE Journal of Research, 1-14. <https://doi.org/10.1080/03772063.2023.2204857>

#### AUTHORS:



**Ali Wassouf** received a master's degree in electrical engineering from Marwadi University, Rajkot, India and received PhD degree in Electronics and Communication Engineering from Shoolini University,

Himachal Pradesh, India. His areas of research are Electronics and Communication Engineering. He can be contacted at

**Email:** [awass3050@gmail.com](mailto:awass3050@gmail.com)



**Raj Kumar Saini**, received PhD degree in power. He has been working as an Associate Professor in the Department of Electronics and Communication Engineering at Shoolini University, India. Her areas of research are Electronics and Communication Engineering.

**Email:** [rksaini@shooliniuniversity.com](mailto:rksaini@shooliniuniversity.com)